

Motor neuron degeneration in a mouse model of seipinopathy

J Guo^{1,2}, W Qiu¹, SLY Soh¹, S Wei¹, GK Radda¹, W-Y Ong², ZP Pang^{*,3} and W Han^{*,1,4,5,6}

Heterozygosity for missense mutations (N88S/S90L) in *BSCL2* (Berardinelli–Seip congenital lipodystrophy type 2)/*Seipin* is associated with a broad spectrum of motoneuron diseases. To understand the underlying mechanisms how the mutations lead to motor neuropathy, we generated transgenic mice with neuron-specific expression of wild-type (tgWT) or N88S/S90L mutant (tgMT) human *Seipin*. Transgenes led to the broad expression of WT or mutant *Seipin* in the brain and spinal cord. tgMT, but not tgWT, mice exhibited late-onset altered locomotor activities and gait abnormalities that recapitulate symptoms of seipinopathy patients. We found loss of alpha motor neurons in tgMT spinal cord. Mild endoreticular stress was present in both tgMT and tgWT neurons; however, only tgMT mice exhibited protein aggregates and disrupted Golgi apparatus. Furthermore, autophagosomes were significantly increased, along with elevated light chain 3 (LC3)-II level in tgMT spinal cord, consistent with the activation of autophagy pathway in response to mutant *Seipin* expression and protein aggregation. These results suggest that induction of autophagy pathway is involved in the cellular response to mutant *Seipin* in seipinopathy and that motoneuron loss is a key pathogenic process underlying the development of locomotor abnormalities.

Cell Death and Disease (2013) 4, e535; doi:10.1038/cddis.2013.64; published online 7 March 2013

Subject Category: Experimental medicine

Seipin proteins, encoded by the Berardinelli–Seip congenital lipodystrophy type 2 (*BSCL2*) gene in human, are endoreticular (ER) membrane proteins consisting of 398 (short-form) or 462 (long-form) amino acids.^{1–3} The long form is the predominant form in human.⁴ Loss of *Seipin* functions due to null mutations or premature stop codon mutations is associated with a rare autosomal-recessive form of lipodystrophy, which is characterized by severe lipoatrophy, insulin resistance and hypertriglyceridemia.^{5,6} Two defined missense mutations in the *BSCL2* gene that disrupt the N-glycosylation motif (N–X–S/T), namely N88S and S90L, are associated with a number of motor neuron diseases, including distal hereditary motor neuropathy type V and Silver syndrome/spastic paraplegia 17.^{1,7,8} Both upper and lower motor neurons, and peripheral motor axons are differentially affected in patients with these mutations.^{9,10} The broad spectrum of *Seipin*-related motor neuron diseases is collectively referred to as seipinopathy.^{3,9–11} There is no effective treatment option for seipinopathy due to incomplete understanding of the pathogenesis of the disease.

Previous studies reported that the N88S/S90L mutations resulted in the formation of cytoplasmic inclusions and

enhanced ubiquitination, leading to unfolded protein accumulation in the ER and eventually ER-stress-associated cell death.^{2,3,8,12} A recent report using a transgenic mouse model overexpressing N88S mutant *Seipin* suggested that ER stress, but not neuronal loss, was one of the key pathogenic processes.¹³ As the proposed ER-stress model was based on either *in vitro* results or a mouse study that compared the mutant transgenic mouse line with non-transgenic wild-type (WT) mice as controls, instead of with a transgenic mouse line overexpressing WT *Seipin*, it was unclear whether ER stress was simply the result of protein overexpression of the transgene or specific to the mutant *Seipin* in the mutant transgenic line. Therefore, the underlying mechanism of how mutant *Seipin* leads to motor neuron dysfunction remains enigmatic.

In this study, we generated transgenic mouse models with neuron-specific overexpression of either WT (tgWT) or N88S/S90L mutant (tgMT) human *Seipin*. Remarkably, similar to motor neuron diseases such as familial amyotrophic lateral sclerosis (fALS), tgMT mice developed late-onset progressive motor phenotypes related to both upper and lower motor neurons, reminiscent of seipinopathy. We found that mutant

¹Laboratory of Metabolic Medicine, Singapore Bioimaging Consortium, Agency for Science, Technology and Research (A*STAR), Singapore, Singapore; ²Department of Anatomy, National University of Singapore, Singapore, Singapore; ³Child Health Institute of New Jersey, Department of Neuroscience and Cell Biology, Robert Wood Johnson Medical School, 89 French Street, New Brunswick, NJ, USA; ⁴Metabolism in Human Diseases, Institute of Molecular and Cell Biology, Agency for Science, Technology and Research (A*STAR), Singapore, Singapore; ⁵Department of Biochemistry, Yong Loo Lin School of Medicine, National University of Singapore, Singapore, Singapore and ⁶Program in Cardiovascular and Metabolic Disorders, Duke-NUS Graduate Medical School, Singapore, Singapore

*Corresponding author: ZP Pang, Child Health Institute of New Jersey, Department of Neuroscience and Cell Biology, Robert Wood Johnson Medical School, 89 French Street, New Brunswick, NJ 08901, USA. Tel: + 732 235 8074; E-mail: pangzh@umdnj.edu.

or W Han, Laboratory of Metabolic Medicine, Singapore Bioimaging Consortium, 11 Biopolis Way, No. 02-02 Helios, Singapore 138667, Singapore.

Tel: + 65 6478 8721; Fax: + 65 6478 9957; E-mail: weiping_han@sbic.a-star.edu.sg

Keywords: autophagy; motor neuron loss; neuron-specific expression; protein aggregates

Abbreviations: ALS, amyotrophic lateral sclerosis; *BSCL2*, Berardinelli–Seip congenital lipodystrophy type 2; GA, Golgi apparatus; GFAP, glial fibrillary acidic protein; LC3, microtubule-associated protein 1 light chain 3; tgMT, mutant transgenic; tgWT, wild-type transgenic; UPR, unfolded protein response

Received 06.12.12; revised 30.1.13; accepted 07.2.13; Edited by A Verkhatsky

Seipin formed protein aggregates in the CNS neurons of tgMT mice and caused a specific loss of alpha motor neurons in the ventral horn of spinal cord. There was no obvious upregulation of ER-stress or inflammation markers in tgMT mice when compared with tgWT mice. Surprisingly, an increase of autophagosomes, along with an increase of LC3-II level, was detected in the spinal cord of tgMT mice, consistent with the activation of autophagy pathway. Taken together, these results suggest autophagy and motor neuron loss, but not ER stress, as key pathogenic processes underlying seipinopathy development.

Results

Generation of transgenic mice expressing WT or N88S/S90L mutant human Seipin. Although both N88S and S90L mutations disrupt N-glycosylation of Seipin, patients carrying either N88S or S90L mutation exhibit different subtypes of motor neuropathy phenotypes.^{14,15} To establish an animal model to study a wide range of seipinopathy, we generated a transgenic mouse line with neuron-specific expression of N88S/S90L double mutant human Seipin under the control of Thy1.2 promoter, along with a control mouse line expressing WT human Seipin under the same promoter (Figure 1a).^{16,17} Similar strategy to harness synergistic effects of mutations was adopted in mouse models of Parkinson disease¹⁸ and Alzheimer disease.¹⁹ The coding sequence for the Myc–human Seipin fusion protein was placed upstream of an IRES (internal ribosome entry site)–GFP cassette, followed by hGH poly-A and SV40 enhancer (Figure 1a). We established transgenic mouse lines by backcrossing the founders to B6C3F1 hybrid mice, and selected the mouse line with highest expression levels of WT (tgWT) or N88S/S90L mutant (tgMT) Seipin in the central nervous system (CNS) (Figure 1b). The expression of exogenous Seipin (anti-myc) and endogenous Seipin (anti-Seipin) was similar in the cortex of transgenic animals (Figures 1c–e). The mutant Seipin formed cytoplasmic protein aggregates in tgMT CNS as reported previously (Figure 1e).^{2,3,8}

N88S/S90L mutant Seipin transgenic mice develop locomotor deficits. We first measured the body weight of transgenic animals, and found that both tgWT and tgMT mice showed similar body weight as their non-transgenic littermates at all age points tested (Figure 2a). We next examined the metabolic indices of these animals by using a Comprehensive Lab Animal Monitoring System (CLAMS). Six pairs of tgMT or tgWT mice and their non-transgenic littermates between 8 and 9 months of age were measured over a 6-day period after 1 day of acclimatization. We found no deficits in metabolic parameters, including basal metabolic rate (BMR; measured by basal oxygen consumption), respiratory exchange rate (RER) or food intake in the transgenic mice (data not shown). Remarkably, tgMT mice showed significantly increased vertical activities at both day- and nighttime compared with their non-transgenic littermates, whereas no such difference was observed between tgWT mice and their control littermates (Figure 2b). These findings indicate that the change in locomotor activities of tgMT mice was not due

to a nonspecific effect of protein overexpression, but a consequence of mutant Seipin expression.

To evaluate whether the transgenic mice recapitulate behavioral phenotypes of seipinopathy patients, we examined hand muscle strength by grip strength test and gait ataxia by footprint analysis in the transgenic mice and their respective non-transgenic littermate controls. Compared with their littermate control and tgWT mice, tgMT mice showed significantly decreased grip strength (Figure 2c), indicating the onset of hand muscle weakness due to lower motor neuron disturbance. For footprint analysis, we measured stride length and base width to detect ataxic gait, and the overlap between forepaw and hindpaw placement to assess the accuracy of foot placement and the uniformity of step alternations.²⁰ We recorded these parameters for a group of 11- to 12-month-old tgMT mice and their control littermates on a paper runway (Figure 2d), and measured the stride length, base width and overlap for each mouse (Figure 2e). Compared with control, tgMT mice exhibited abnormal gait, as evidenced by increased forelimb and hindlimb stride lengths (Figure 2f), suggesting abnormalities of upper motor neurons in tgMT mice. These results indicated that the onset of motor phenotypes was slowly progressive in tgMT mice as weakness in grip strength could be detected only after 8 months of age and gait abnormalities 11–12 months of age. In contrast, no significant gait abnormality was observed in tgWT mice (Supplementary Figure S1). These results demonstrate that the late-onset and progressive distal motor dysfunction in tgMT mice mimic those of human patients with seipinopathy.²¹

Mutant Seipin forms aggregates in the CNS of tgMT mice. Motor behavioral dysfunction disease, such as fALS, is often associated with dysfunction and/or loss of motor neurons.^{22–24} We examined the histology of the spinal cord by Nissl staining in tgMT mice, and compared with their non-transgenic littermates and tgWT mice. We noticed the appearance of cytoplasmic vacuolization and cellular swelling in the motor neurons of tgMT mice, but not in non-transgenic or tgWT mice (Figure 3a), indicating that the tgMT motor neurons might be undergoing degeneration.²⁵ We then performed immunofluorescence study using anti-Myc antibody to visualize the transgenic expression of mutant and WT Seipin. Similar to the findings in the cortical neurons of tgMT mice (Figure 1e), we observed protein aggregates widely present in the spinal cord motor neurons in ~7-month-old tgMT mice (Figure 3b). Approximately 20% cortical and 40% spinal neurons of tgMT mice were found to contain Seipin aggregates, while none in non-transgenic control or tgWT mice (Figure 3c). To assess the onset of Seipin aggregates, we also examined the transgenic mice at ~1 month of age. Cytoplasmic mutant Seipin aggregates were present in very few cortical neurons, but in many spinal cord motor neurons (data not shown), indicating that mutant Seipin aggregates form early in life.

Reduced number of alpha motor neurons in the CNS of tgMT mice. We noticed in the histological examination by Nissl staining that there appeared to be fewer motor neurons in the tgMT mice, especially those with large cell bodies, so

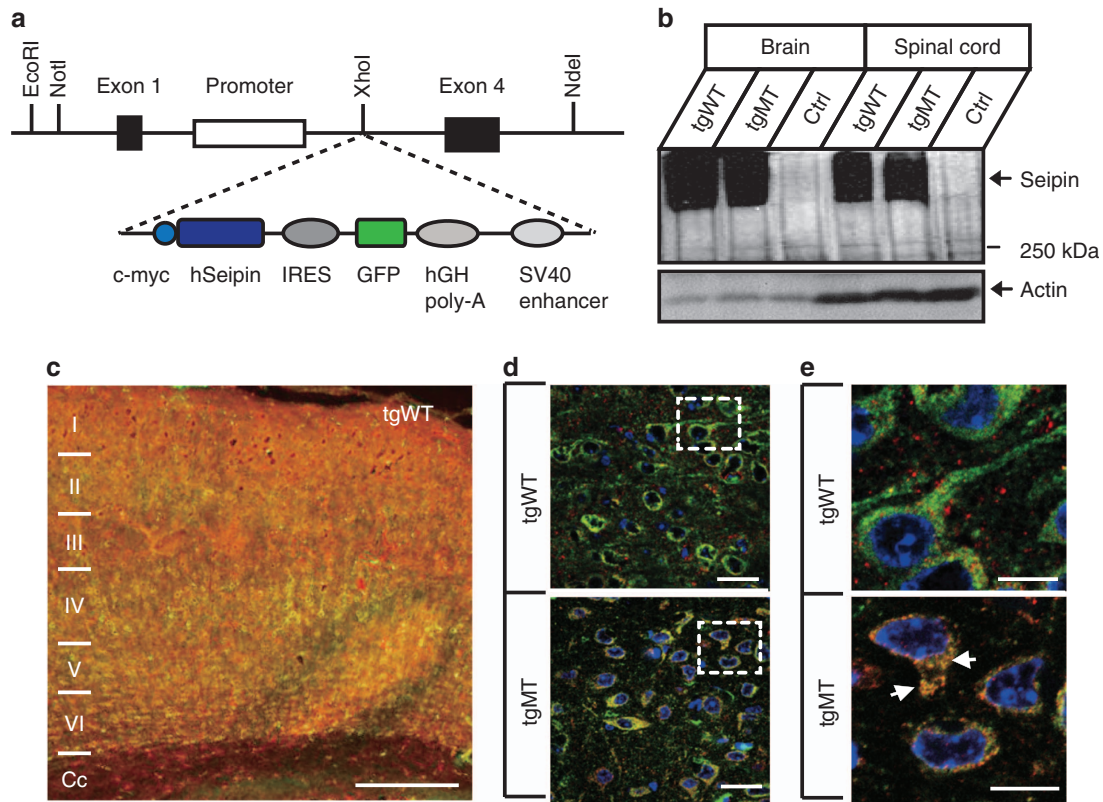


Figure 1 Generation of transgenic mice expressing WT or N88S/S90L double mutant human Seipin. (a) Diagram of transgenic vector for neuron-specific expression of WT or N88S/S90L double mutant human Seipin. The coding sequences of Myc-tagged Seipin and GFP was separated by the IRES sequence and followed by hGH polyadenylation sequence and SV40 enhancer. (b) Transgenic Seipin expression in the CNS of tgWT and tgMT mice was detected by using anti-Myc antibody. Myc-Seipin was detected as high-molecular-weight protein aggregates (over 250 kDa). (c) Transgenic Seipin was broadly expressed in the cortex of tgWT (c) and tgMT mice (not shown). (d and e) Double-labeling of transgenic Seipin (by anti-Myc antibody, green) and total Seipin (anti-Seipin antibody, red) showed apparent colocalization of the transgenic and the endogenous Seipin in neurons at layer IV of the cortex. Blue: 4',6-diamidino-2-phenylindole (DAPI). Cytosolic protein aggregates (arrows) were found only in the neurons of tgMT mice (e), but not in tgWT mice (d). Scale bars = 250, 40 and 10 μm for c, d and e, respectively

we quantitated the numbers of motor neurons in Nissl-stained transverse lumbar spinal cord cross-sections (Figure 4a). We did not observe any apparent difference in the total number of motor neurons between tgMT mice and tgWT or control mice (Figure 4c). As neuronal DNA-binding protein NeuN marks alpha but not gamma motor neurons,²⁶ we used anti-NeuN antibody to label specifically alpha motor neurons with large diameters and noticed that the number of alpha motor neurons was significantly reduced in the spinal cord of tgMT mice (Figures 4b and c). These results suggest that mutant Seipin specifically affects alpha motor neurons in the spinal cord of tgMT mice, which may lead to the development of locomotor dysfunctions.

Slight increase in ER-stress and inflammatory responses in both tgMT and tgWT mice. Previous *in vitro* studies suggested that mutations at the N-glycosylation site of Seipin caused accumulation of misfolded protein in the ER, leading to the induction of ER stress and unfolded protein response (UPR) and eventually cell death.^{12,27} Therefore, we tested this hypothesis in the CNS of tgWT and tgMT mice. As UPR and inflammatory responses are intimately connected,^{28,29} we analyzed the mRNA levels of well-established ER-stress markers BiP and CHOP, major inflammatory cytokines TNF- α and IL-6 and inflammatory

mediators iNOS and COX2. Unexpectedly, most of these genes showed similar expression levels in the CNS of tgWT, tgMT and their control mice. In both tgWT and tgMT mice, BiP expression was increased in the spinal cord, but unaltered in the brain when compared with control mice (Figures 5a and b). We also performed immunoblots to determine the levels of UPR-responsive proteins BiP, activating transcription factor 4 (ATF4) and activating transcription factor 6 (ATF6).³⁰ Consistent with the qRT-PCR results, BiP was increased in the spinal cord of both transgenic mouse lines when compared with their respective controls (1.5 ± 0.2 - and 1.5 ± 0.1 -fold increase over control for tgWT and tgMT, respectively; $N = 4-5$). No difference was observed between tgWT and tgMT in BiP, ATF4 or ATF6 expression levels (Figures 5c and d). We next examined glial fibrillary acidic protein (GFAP) expression in the lumbar spinal cord sections of transgenic mice by immunohistochemistry (IHC), but found no difference between tgWT and tgMT mice (Figures 5e and f). We also probed GFAP protein expression in the spinal cord by immunoblotting, and there was no difference between the two transgenic mouse lines (Figure 5g). These results suggest that ER stress is similarly induced in tgWT and tgMT mice, which is likely the result of overexpression of the transgenic proteins. Although the upregulation in stress response may have a role in disease

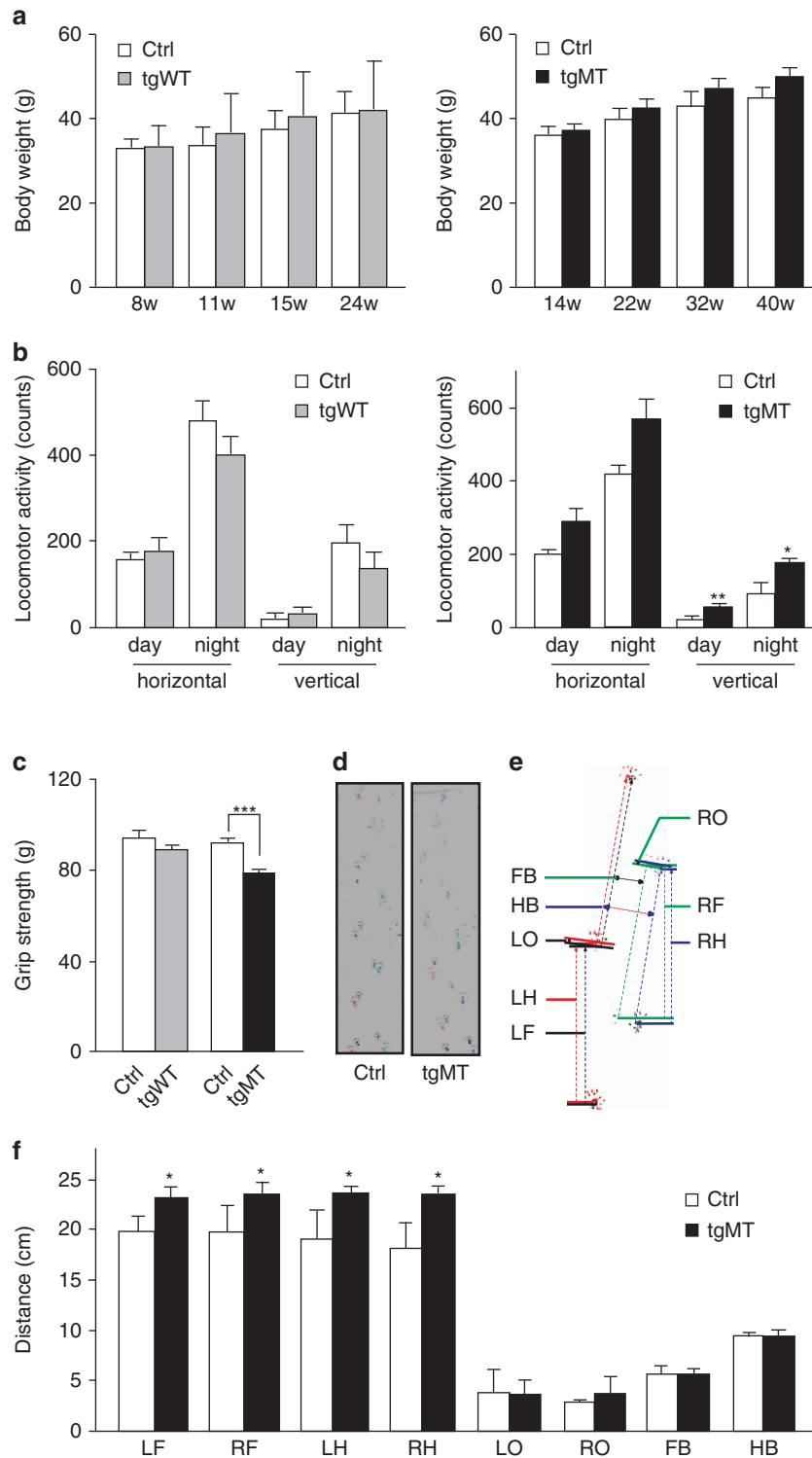


Figure 2 Reduced grip strength and gait abnormality in tgMT mice. **(a)** Normal body weight development in tgWT and tgMT mice. No difference in body weight was observed between tgWT, tgMT and their respective non-transgenic littermates at various time points. $N = 7$ pairs for tgWT and littermate control, and 5 pairs for tgMT and littermate control of 8 months old. **(b)** Locomotor activity of tgWT and tgMT was analyzed in CLAMS. Data were presented as mean \pm S.E.M. $N = 6$ pairs of tgWT or tgMT and control mice. * $P < 0.05$; ** $P < 0.01$. **(c)** Muscle weakness was assessed by analyzing grip strength of tgWT or tgMT mice and their respective non-transgenic littermates. Three consecutive trials were performed for each mouse and the maximal force reached by each animal was recorded. $N = 4$ pairs of tgWT and littermate control, and 4 pairs for tgMT mice and littermate control of 8 months old. *** $P < 0.001$. **(d)** Representative footprints of an 11-month-old tgMT mouse and its control littermate. **(e)** Illustration of standard measurements collected from colored footprints. Ink color for left forelimb: black; right forelimb: green; left hindlimb: red; and right hindlimb: blue. Comparisons of the left and right forelimb stride length (LF and RF), hindlimb stride length (LH and RH), overlap width (LO and RO) and front and hind base width (FB and HB) were made between tgMT and control mice. **(f)** Footprints of tgMT mice showed longer stride lengths compared with control. $N = 9$ for tgMT and 7 for control mice, each was tested in three trials. Data were presented as mean \pm S.E.M.; * $P < 0.05$

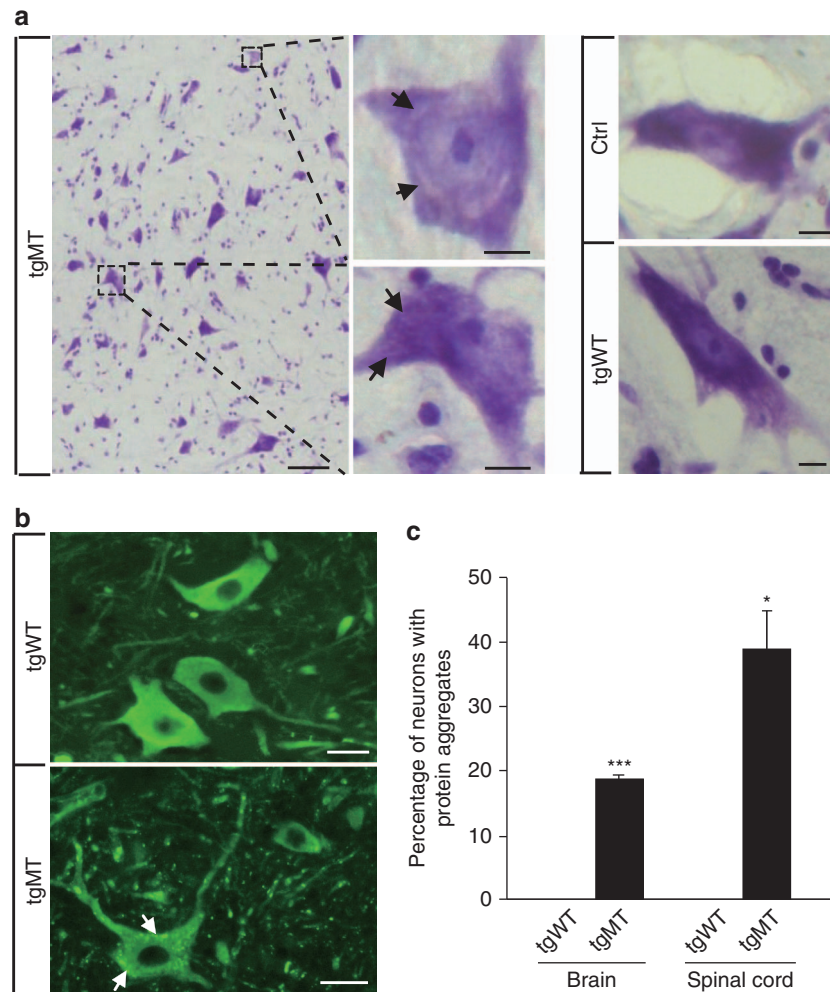


Figure 3 Pathologies of spinal cord motor neuron in tgMT mice. (a) Nissl staining of the motor neurons in lumbar spinal cord cross-sections of 7-month-old tgMT, tgWT and control mice. Enlarged image of the encircled area revealed cytoplasmic vacuolization and cellular swelling in alpha motor neurons of tgMT mice, while no sign of neuronal degeneration was found in the spinal cord of tgWT or control mice. Scale bars = 50 μ m in overview and 5 μ m in enlarged images. (b) Immunostaining with anti-Myc antibody showed aberrant intracellular Seipin aggregates (arrows) in the spinal cord cross-sections of tgMT, but not in tgWT mice. Scale bars = 20 μ m. (c) Percentage of the neurons with intracellular Seipin aggregates in the brain or spinal cord of tgWT or tgMT mice. Seipin aggregates were found only in the CNS of tgMT mice, but not in tgWT mice. * $P < 0.05$; *** $P < 0.001$

progression, it is unlikely that this is the major pathogenic factor responsible for the development of locomotor deficits in tgMT mice.

Fragmentation of the Golgi apparatus in the spinal cord motor neurons of tgMT mice. To further evaluate the pathology responsible for the loss of alpha motor neurons, we performed coimmunostaining of Seipin (using anti-Myc antibody) with various Golgi apparatus (GA) markers and an ER–Golgi transport vesicle marker COPII. In contrast to the defined structures observed in the normal motor neurons in tgWT and control mice, the motor neurons in tgMT mice showed discrete GA fragments and aggregated or dispersed distribution of COPII (Figure 6). We also performed *in vitro* studies using Seipin-overexpressing NSC-34 cells, where GA fragmentation and dispersed COPII staining were found in cells expressing N88S/S90L mutant Seipin (data not shown). These results suggest that motor neurons from tgMT mice may be undergoing cell death.

Activation of autophagy pathway in tgMT mice. Motor neuron diseases have been linked with autophagy, which is critical for misfolded protein degradation, and overactivated autophagic response may result in progressive neurodegeneration.^{31–33} To study whether autophagy was specifically altered in the CNS of tgMT mice, we examined microtubule-associated protein 1 LC3, an established autophagy marker, by immunostaining and immunoblots. Compared with the moderate LC3 staining in control or tgWT mice, the majority of the spinal cord motor neurons of tgMT mice showed a significant increase in LC3 fluorescence, which was well-colocalized with intracellular Seipin aggregates (Figure 7a). Furthermore, the protein levels of LC3-II in the spinal cord of tgMT mice were increased compared with age-matched tgWT mice (Figures 7b and c). In contrast, immunostaining of the brain sections showed no significant changes in the cortical neurons of tgMT mice compared with tgWT mice, implying a spinal motor neuron-specific increase of the LC3 levels (data not shown). To further confirm autophagosome

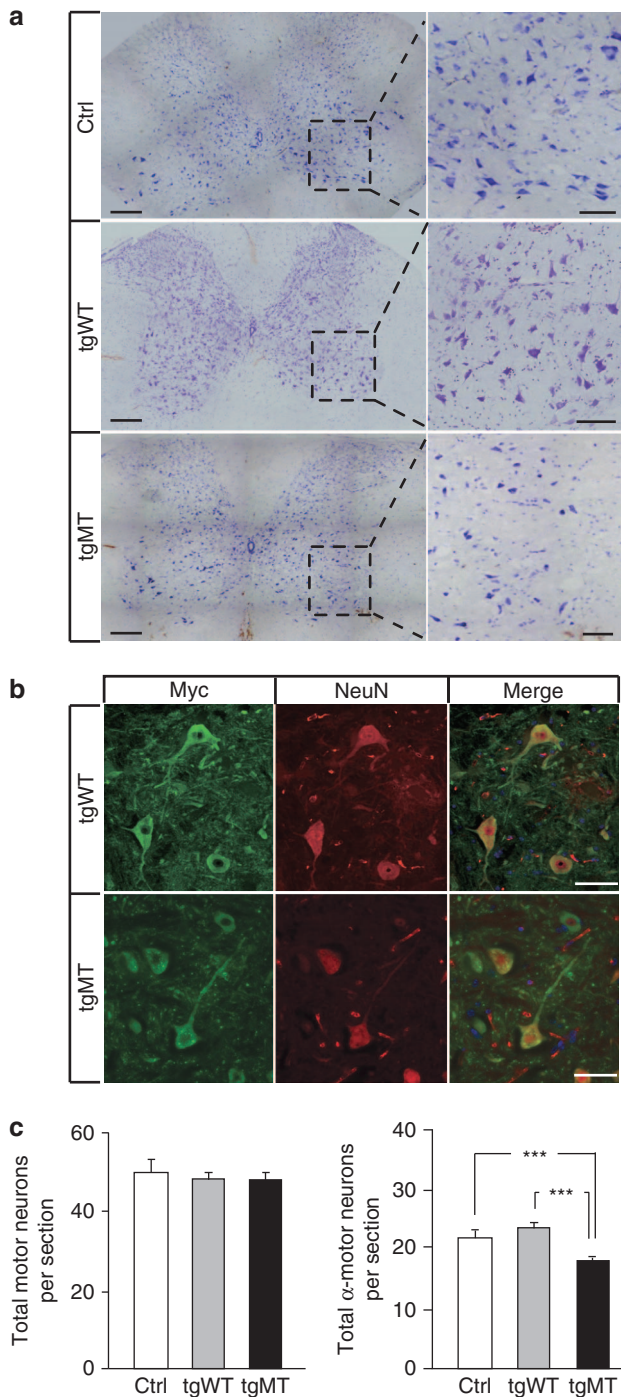


Figure 4 Loss of alpha motor neurons in the spinal cord of tgMT mice. **(a)** Nissl staining of motor neurons in lumbar spinal cord cross-sections of 7-month-old tgWT, tgMT and non-transgenic control mice. Enlarged images of the encircled area revealed reduced number of larger alpha motor neurons in the ventral horn of the spinal cord of tgMT mice compared with tgWT or control mice. Scale bars = 200 μ m. **(b)** Ventral horn of spinal cord sections of tgWT and tgMT mice were stained with anti-Myc (labeling all the motor neurons) and anti-NeuN (labeling alpha motor neurons) antibodies. Scale bars = 50 μ m. **(c)** Quantitation of numbers of all the motor neurons or alpha motor neurons in the ventral horn of lumbar spinal cord sections of tgWT, tgMT and control mice. There was no difference in the number of all the motor neurons, but the number of NeuN-positive alpha motor neurons was significantly reduced in tgMT mice compared with that of tgWT or control mice. *** $P < 0.001$

was induced in the tgMT spinal cord, we performed electron microscopy (EM) analysis of spinal cord cross-sections of 8-month-old tgWT and tgMT mice. Multilamellar, membranous structures were readily detectable in the dendritic neuropil of ventral horn motor neurons of tgMT mice, but not in tgWT mice (Figure 7d). These structures, containing concentric layers of membranes, and sometimes within a vacuole-like structure, were identified as a form of autophagosomes.^{34,35} Compared with the spinal neurons, glial cells in tgMT mice showed few changes, indicating that the changes in tgMT mice were specific to neurons.

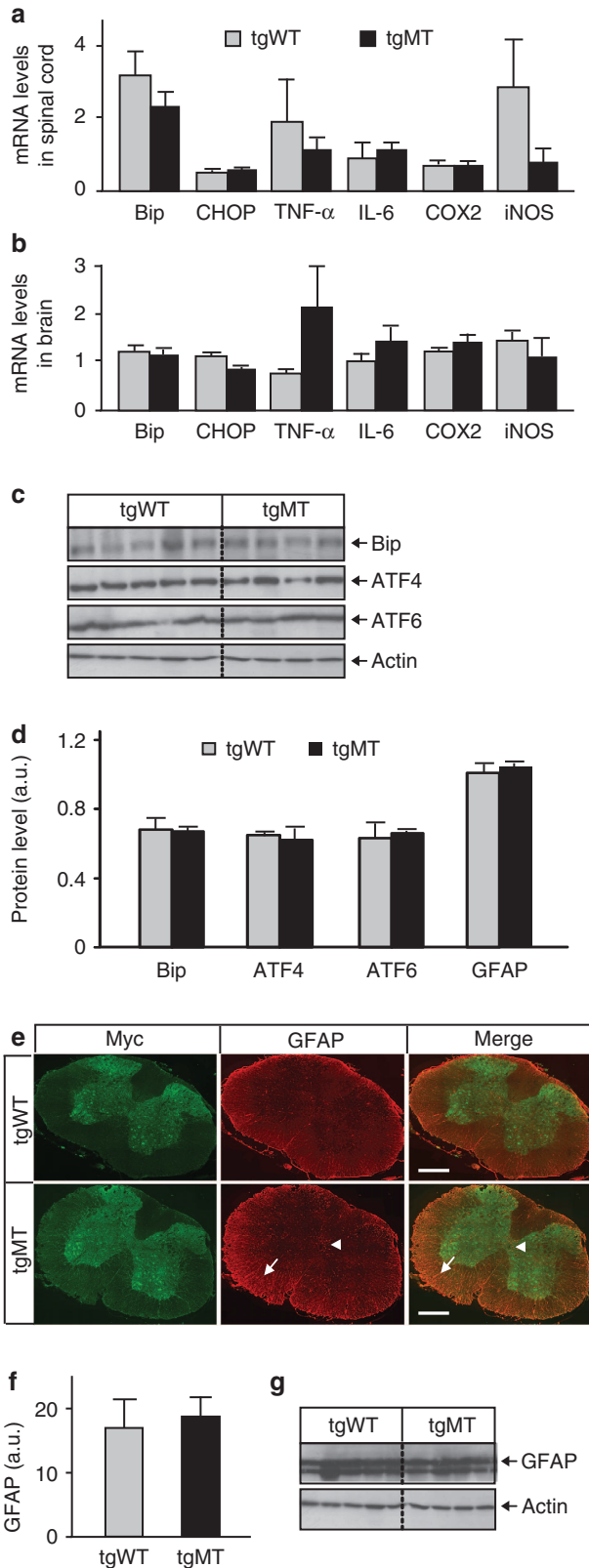
Discussion

This study was aimed to generate a mouse model of seipinopathy and to elucidate the cellular and molecular alternations in the CNS as a result of N88S/S90L mutant Seipin expression, with the view that this would lead to better understanding of the pathological changes in seipinopathy. Our findings demonstrate an association between the neuron-specific overexpression of N88S/S90L mutant human Seipin and progressive motor impairments in tgMT mice. The key pathological features are the formation of mutant protein aggregates and selective loss of alpha motor neurons with increased autophagosomes. As both upper and lower motor neurons are involved in human patients of Seipinopathies, these transgenic mice may serve as a valuable tool for understanding of disease pathology and development of future therapeutic strategies.

Both tgWT and tgMT mice showed high levels of human Seipin overexpression under the control of a neuron-specific promoter in the brain and spinal cord. As expected, tgMT mice exhibited pathologic motor phenotypes, including weaker grip strength, gait ataxia and altered locomotor activities compared with their littermates. These phenotypes recapitulated clinical aspects of patients of Seipinopathies.

A previous study using mutant Seipin transgenic mice reported that the development of progressive motor deficits was associated with ER stress.¹³ In that study, the authors examined expression levels of ER-stress markers BiP and protein disulfide isomerase in the cerebrum by western blots (WBs), and BiP (by using KDEL antibody) and ER-stress signaling molecule X-box binding protein 1 in the spinal cord by IHC, and showed that ER stress was induced in the cerebrum and spinal cord of mutant Seipin transgenic mice. However, comparisons were made between mutant Seipin transgenic mice and non-transgenic control littermates, instead of with WT Seipin transgenic mice. Without testing the WT Seipin transgenic mice, it is not possible to ascertain that the observed differences were the result of mutant Seipin overexpression, and not a nonspecific effect due to the overexpression of an exogenous protein. In this study, we tested for the first time both WT and mutant Seipin transgenic mouse lines. We examined the expression levels of well-established ER-stress and inflammatory markers in tgWT and tgMT mice, but did not detect a significant increase in any of these markers for tgMT when compared with tgWT mice. The mild increase in BiP in the spinal cord for both tgWT and tgMT compared with their control littermates was likely the result of overexpression of human Seipin in these mice, and

not specific to mutant Seipin. And as such, ER stress alone was unlikely the cause for the observed motor deficits in the tgMT mouse line carrying the N88S/S90L double mutations.



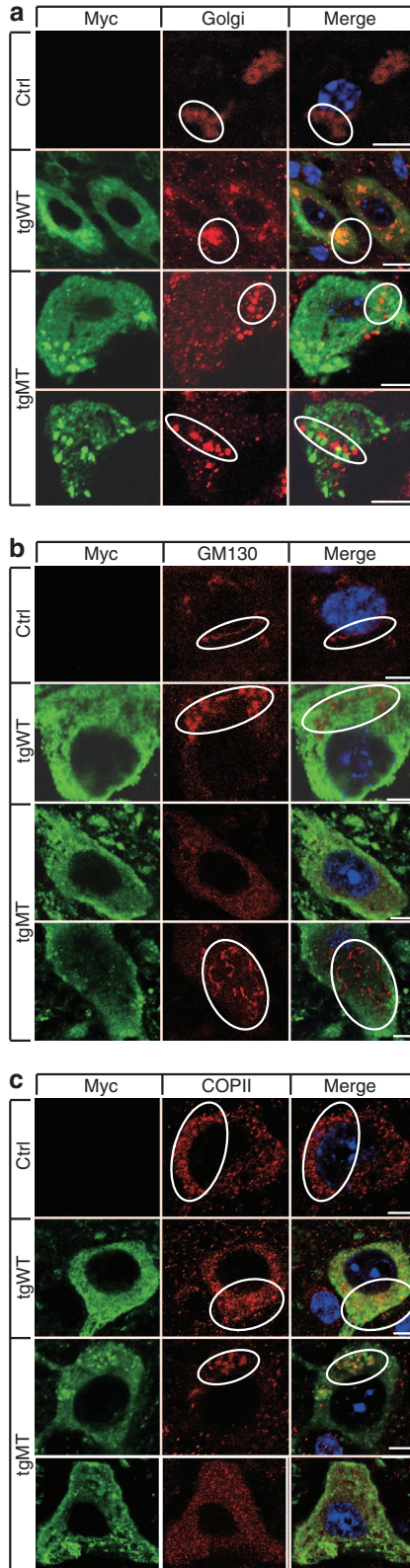
However, we could not rule out the possibility that some pathogenic consequences due to Seipin overexpression, such as ER stress, could still be present in our transgenic mouse lines, or that ER stress might still contribute to the development of motor neuropathy in tgMT mice.

To study the cellular mechanisms underlying the observed motor phenotypes in tgMT mice, we examined neurons in the CNS of tgMT mice. Consistent with previous *in vitro* studies showing that mutant Seipin forms protein inclusions,^{2,3,12} we found that mutant Seipin aggregates were widely distributed in the CNS neurons of tgMT mice. We also detected early pathology during motor neuron disease progression and GA fragmentation in the large spinal motor neurons of tgMT mice.^{25,36–41} Some of the cellular changes, such as Seipin aggregates, could lead to disrupted axonal transport along the neurites. Moreover, we observed selected loss of alpha motor neurons labeled by anti-NeuN antibodies²⁶ in the spinal cord of the tgMT mice. As all these pathological features were present before the onset of major motor phenotypes such as gait ataxia, they likely have roles in the pathogenic process of the motor deficits.

Besides these pathological changes, we identified increased autophagy in the spinal cord of tgMT mice. Autophagy and the ubiquitin–proteasome system are the two major systems for cytoplasmic protein degradation in eukaryotic cells, and alternations to these systems are implicated in neurodegenerative diseases such as Parkinson’s disease, Alzheimer’s disease, Huntington’s disease and ALS.^{31,42} In particular, increased number of autophagosomes has been detected in the spinal motor neurons of ALS and its mouse model.^{43–45} Without compensatory upregulation of degradation systems to clear the autophagic vacuoles, autophagic stress may be developed, which could be detrimental and promote cell death.^{46–48} In this study, we observed increased formation of autophagosome structures only in the spinal cord of tgMT, but not in tgWT mice. Notably, EM studies did not reveal significant signs of apoptosis in tgMT mouse spinal cord sections, supporting the insidious and slow-progressing nature of neuronal degeneration and death associated with the late onset of motor phenotypes in our tgMT mice. We suggest that such chronic pathogenic

Figure 5 Elevated ER stress in the CNS of tgWT and tgMT mice. **(a, b)** Expression of ER stress and inflammation indicators in the spinal cord **(a)** and brain **(b)** was assessed by quantitative RT-PCR. The relative expression levels in tgWT and tgMT mice were normalized to their respective non-transgenic littermates (expression level set as 1). $N = 4$ pairs for 7-month-old tgWT and littermate controls, and 4 pairs for tgMT and littermate controls of the same age. **(c)** Expression of ER-stress-mediating proteins in the spinal cords of 7-month-old tgWT ($N = 5$) and tgMT ($N = 4$) mice. **(d)** Quantification of WBs after normalization to actin (arbitrary unit, a.u.). No significant difference in Bip, ATF4, ATF6 and GFAP levels was found in the spinal cord of tgWT and tgMT mice. **(e)** Immunostaining of GFAP in the spinal cord cross-sections of 7-month-old tgWT and tgMT mice. Signals were mainly from the fibers in the white matter (arrows), and to a much lesser extent, from astrocytes in the gray matter (arrowheads). TgWT and tgMT mouse spinal cords showed similar GFAP expression. Scale bars = 500 μ m. **(f)** Fluorescence intensity of GFAP staining showed a comparable level between tgWT and tgMT mice. **(g)** WBs showed similar GFAP expression in the spinal cord of tgWT and tgMT mice. COX, cyclooxygenase; IL, interleukin; iNOS, inducible nitric oxide synthase; TNF, tumor necrosis factor

progress could be associated with the accelerated autophagic removal of mutant Seipin aggregates and associated structures in spinal motor neurons.



Taken together, the neuron-specific overexpression of N88S/S90L mutant Seipin leads to slowly progressive upper and lower motor neuron pathologies reminiscent of phenotypes in seipinopathy patients. Seipin aggregates result in a series of pathological changes in the neurons, including GA fragmentation. Such changes may eventually lead to the loss of alpha motor neurons in tgMT mice, and the ensuing motor phenotypes. Importantly, we show that activation of autophagic response instead of elevation of ER stress or inflammatory response is specifically involved in this process. The increased autophagic activity may be a compensatory response to accelerate the removal of mutant Seipin aggregates and to protect motor neurons from apoptosis, and thus delaying the progression of motor phenotypes. On the other hand, excess autophagy may also be detrimental to neurons.^{48,49} Our novel mouse model of motor neuropathy will allow future studies to investigate pathogenic mechanism of Seipin mutations, and may be valuable for developing therapeutic strategies for seipinopathy and other motor neuron diseases.

Materials and Methods

Animal welfare. All experiments involving animals were reviewed and approved by Institutional Animal Care and Use Committee of Agency for Science, Technology and Research (A*STAR) in Singapore (IACUC nos. 080351 and 090428). All mice used in this study were bred and housed in the animal facility. They were maintained at $25 \pm 1^\circ\text{C}$ on a 12 h/12 h light/dark cycle (0700–1900 h), and allowed free access to water and rodent chow (15% kcal from fat; Harland Tekland, Madison, WI, USA). Transgenic mice were bred with non-transgenic WT mice, and age- and gender-matched non-transgenic mice from such breeding were used as controls to the transgenic mice in all the experiments.

Construction of plasmids. To generate Myc-tagged Seipin in an expression vector, full-length mouse WT Seipin (WT-Seipin) was cloned into pCMV5-Myc by inserting the PCR product using mouse Seipin cDNA (Addgene, Cambridge, MA, USA) as the template with the following primers: 5'-GCCAATTGGCATGATACATCAAAGAAGAG-3' and 5'-GGAGATCTTCAG-GAAGCTGGAGCAGGTC-3'. DNA sequence containing Myc-tagged WT-Seipin was cut out from the resulting vector and inserted into lentiviral expression vector L309. Site-directed mutagenesis to introduce N88S/S90L mutations to these WT-Seipin constructs was carried out by using a QuikChange II XL Site-Directed Mutagenesis Kit (Stratagene, La Jolla, CA, USA). All the DNA plasmids used in this study were verified by sequencing.

Generation of WT and N88S/S90L mutant transgenic mice. The Thy1-Myc-Seipin transgene, containing the human WT-Seipin or N88S/S90L mutant Seipin (Mut-Seipin) cDNA under the control of the mouse Thy1 promoter, was constructed by placing the 2.7-kb Myc-Seipin-IRES-GFP, hGH polyadenylation signal and SV40 enhancer cassette into *XhoI* site of the pThy1 transgenic vector by blunt ligation (Figure 1a). The purified linear transgenic vector was injected into fertilized oocytes using standard techniques.⁵⁰ Transgenic founders were identified by genotyping from tail DNA using the following primer pair: 5'-CCTTATTCCAAGCGGCTTC and 5'-GACTATGCGGAGTTGACTCC, and bred to B6C3F1 hybrid mice to establish independent transgenic lines. The transgenic lines with the highest expression levels of WT-Seipin (tgWT) or Mut-Seipin (tgMT) were selected for further studies.

Figure 6 Fragmentation of the GA in the motor neurons of tgMT mouse spinal cords. Cross-sections of 7-month-old tgWT, tgMT and non-transgenic control (Ctrl) mouse spinal cord was colabeled with anti-Myc antibody for transgenic Seipin (green) and anti-Golgi (a), GM130 antibody against GA (b) or COPII antibody against transport vesicles from rough ER to GA (c). In contrast to the well-defined structures in the motor neurons of tgWT or control mice, the motor neurons in tgMT mice showed discrete GA fragments, and aggregated or dispersed distribution of COPII vesicles (circles). Scale bars = 10 μm

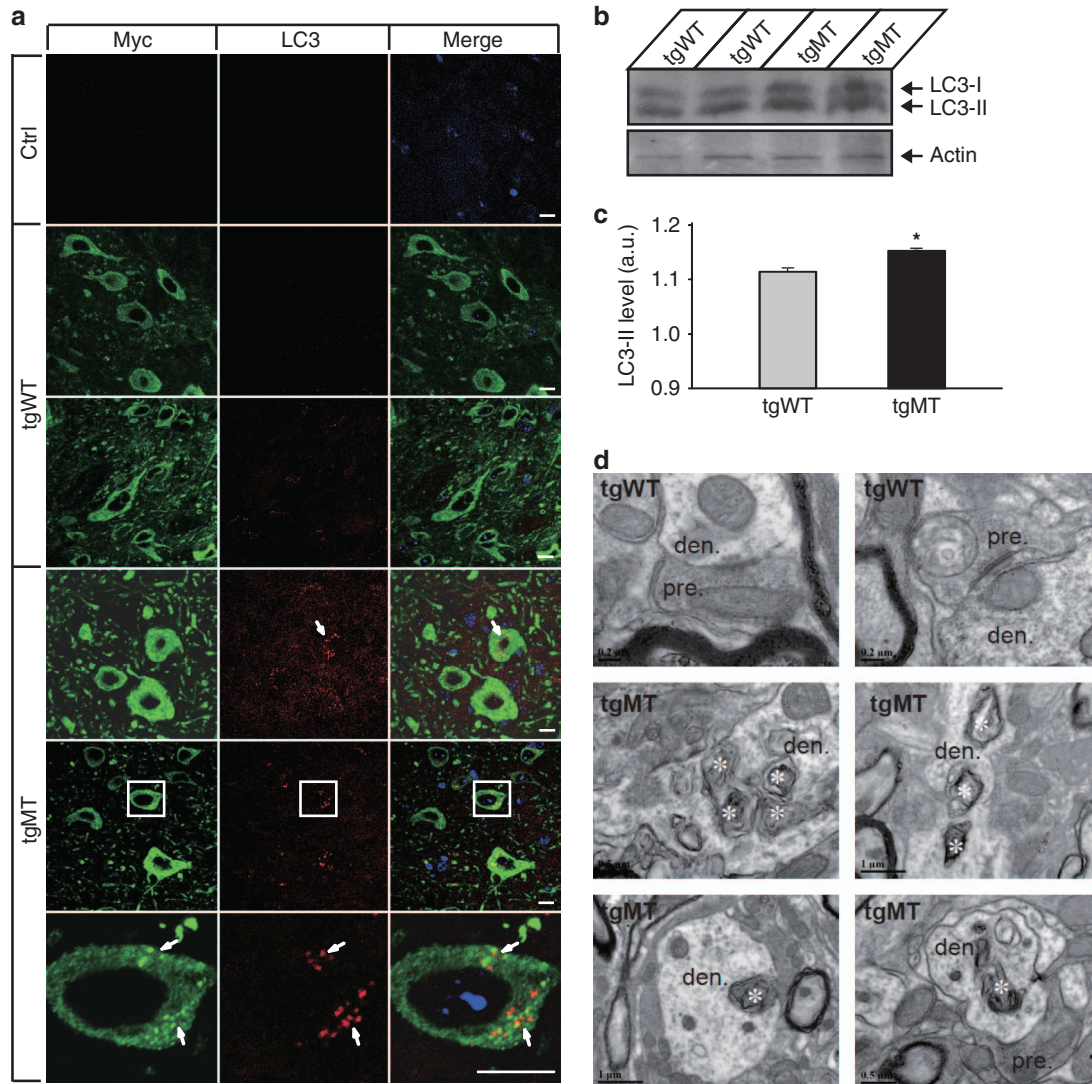


Figure 7 Activation of autophagy responses in the CNS of tgMT mice. (a) Immunostaining of LC3 as a marker for autophagy activation in the spinal cord of 7-month-old tgWT, tgMT or control mice. The spinal cord motor neurons in tgMT mice showed increased LC3 staining, which was partially colocalized with mutant Seipin aggregates. Green: Myc; red: LC3. Scale bars = 10 μ m. (b) LC3-II expression was significantly increased in tgMT mouse spinal cord compared with tgWT or control mice. (c) Actin-normalized LC3-II levels in the spinal cord of tgMT mice were increased compared with tgWT mice. (d) EM of the spinal cord cross-sections of transgenic mice. Asterisk indicates the formation of multilamellar membranous structures only in the dendrites (labeled as 'den.') of tgMT mice, which is a form of autophagosomes. Axon terminals that formed synapses near the sites of dendritic multilamellar bodies (labeled as 'pre.') contained gray cytoplasm with few synaptic vesicles compared with the normal axon terminals with clear cytoplasm in tgWT mice

RNA isolation, reverse transcription and quantitative real-time PCR analysis. Gene expression was assessed by quantitative real-time PCR analysis as described previously.⁵¹ Briefly, total RNA was extracted from tissues by TRIzol method (Invitrogen, Carlsbad, CA, USA). RNA samples were treated with DNase and reverse transcribed using random hexamer primers. The cDNAs were then used for qPCR analysis in triplicates. Primer sequences used for q-PCR were 5'-CCGTCTACAGAAAAGGTAGAC-3' and 5'-GCAGCAGCTGGTGGTTC CTC-3' for human Seipin, and 5'-TCCGACAAAGGGATAACTACA-3' and 5'-GTAGATTCCTGACCTGGCTGATG-3' for mouse Seipin.

Oxymax/CLAMS. Oxymax/CLAMS (Columbus Instruments, Columbus, OH, USA) was used to measure individual mouse on their oxygen consumption (VO_2), carbon dioxide production (VCO_2), activities and food intake essentially as described previously.⁵² Six pairs of tgMT and control littermates were used for measurements at 5 months of age and later at 8–9 months of age, and six pairs of tgWT mice and control mice were examined at 8–9 months of age. Mice were individually housed at 24 ± 1 °C, and given free access to chow and water. All the

measurements were taken every 15 min for 6 days after the mice were acclimatized for 1 day. BMR was determined by averaging lowest plateau region of oxygen consumption curve corresponding to resting periods. The RER was calculated as the ratio between VCO_2 and VO_2 . X total, X ambulatory and Z total movements were a tally of the number of times the motion sensors detected for horizontal, ambulating and vertical movement, respectively. All data collected were averaged from 6 days' monitoring.

Grip strength. Grip strength of the forelimbs of transgenic mice was measured as described previously.⁵³ Briefly, 8-month-old tgWT or tgMT mice with their non-transgenic littermates, respectively, were brought to the testing room and allowed to acclimatize for 10 min before the test began. A grip strength meter (Columbus Instruments) was used to measure the forelimb grip strength of each mouse. Mice were held by the tail and allowed to place their forelimbs on the smooth metal pull bar connected to the force sensor, and then slowly pulled away until they released the bar. Untrained mice were tested three times without rest and the maximal force reached by each animal (in grams) was recorded.

Footprint analysis. To assess the locomotion of transgenic mice, we performed footprint analysis using an adapted open-top runway system.^{7,54} Briefly, tgMT mice and their non-transgenic littermates of 11–12 months old were analyzed once per week for three consecutive weeks. Mice were allowed to habituate the 10 × 50 cm² walkway with a dark enclosed goal box at the end and then trained to walk steadily through the walkway. Each paw of a mouse was then dipped into non-toxic inkpads for labeling with a different color and footprints were then collected on paper spread on the floor of the walkway. Stride length, base length and overlap length were measured in 3–5 consecutive footprints of each animal.

Immunoblot analysis. Mouse tissue samples were resolved by SDS-PAGE and transferred to nitrocellulose membrane (Invitrogen), followed by specific primary antibodies and HRP-conjugated secondary antibodies. The proteins of interest were detected by ECL Western Blotting Detection Reagents (GE Healthcare, Buckinghamshire, UK) according to the manufacturer's instructions.

Histological studies. Mice used for IHC studies were ~7 month old, unless specified otherwise. Freshly harvested mouse brain and spinal cords were fixed with 4% paraformaldehyde overnight, and then transferred to 30% sucrose in 0.1 M PBS for at least 24 h before OCT embedding. The 10- μ m-thick cryosections were prepared for immunostaining. After permeabilization by 0.5% Triton X-100 in PBS for 10 min, sections were blocked with blocking buffer containing 2% BSA in PBS for 30 min, incubated with primary antibodies in blocking buffer for 1 h at room temperature, followed by fluorescein-conjugated secondary antibodies for another 1 h. Cryosections were then mounted using Vectasheild HardSet Mounting Medium with DAPI (Vector Labs, Burlingame, CA, USA) and images were collected by using a Nikon 90i or A1R Spectral Confocal microscope (Tokyo, Japan). For Nissl staining, motor neurons were counted in every 10th section of the lumbar spinal cord (L1–L6) from at least six pairs of tgWT or tgMT mice and their respective non-transgenic littermates. Neurons were stained with cresyl violet, and the number of total motor neurons and NeuN staining positive alpha motor neurons in the anterior horns were determined according to the previously described morphological criteria, where alpha motor neurons in the gray matter at the ventral horn were identified by their large size (nuclear diameter >9–10 μ m; cell body diameter >20 μ m).⁵⁵

Antibodies. Primary antibodies for IHC, immunocytochemistry (ICC) or WB used in this study were: mouse 9E10 anti-c-Myc (Santa Cruz Biotechnology, Santa Cruz, CA, USA; IHC/ICC, 1:100; WB, 1:1000); mouse anti- β -actin (Santa Cruz Biotechnology; WB, 1:3000); anti- γ -tubulin (Sigma, St. Louis, MO, USA; WB: 1:1000); mouse anti-GFAP (Sigma; IHC, 1:100; WB, 1:1000); mouse anti-GM130 (BD Transduction Laboratories, San Jose, CA, USA; IHC, 1:100); mouse anti-NeuN antibody (Millipore, Billerica, MA, USA; IHC, 1:100); mouse anti-microtubule-associated protein 2 (Millipore; ICC, 1:100); mouse anti-KDEL (Abcam, Cambridge, MA, USA; IHC, 1:100); rabbit anti-Myc (Millipore; IHC, 1:100); rabbit anti-Seipin serum by rabbit immunization (IHC, 1:100); rabbit anti-BiP/Grp78 (Cell Signaling Technology, Beverly, MA, USA; WB, 1:1000); rabbit anti-ATF4 or -ATF6; Santa Cruz Biotechnology; WB, 1:1000); rabbit anti-LC3 (MBL, Woods Hole, MA, USA; ICC, 1:100); rabbit anti-58K Golgi protein (Abcam; ICC, 1:100); rabbit anti-COPII (Thermo Scientific, West Palm Beach, FL, USA; IHC, 1:100); and rabbit anti-calnexin (Abcam; IHC, 1:100).

Electron microscopy. Electron microscopy was carried out by subdissecting the spinal cords sections (L4–L5) into smaller rectangular portions. The sections were osmicated, dehydrated in an ascending series of ethanol and acetone, and embedded in Araldite. Thin sections were obtained from the first 5 μ m of the sections, mounted on copper grids coated with Formvar and stained with lead citrate. They were viewed on a Philips EM208 electron microscope (Hillsboro, OR, USA).

Statistical analysis. Data were reported as mean \pm standard error of the mean. One-way ANOVA followed by Bonferroni's *post hoc* test or F-test was used to determine significant differences ($P < 0.05$) between groups.

Conflict of Interest

The authors declare no conflict of interest.

Acknowledgements. This study was supported by intramural funding from Agency for Science, Technology and Research (A*STAR) Biomedical Research Council (W.H.); Robert Wood Johnson Foundation to CHINJ and Brain and Behavioral Research Foundation NARSAD Young Investigator Award (Z.P.P.). We thank C. Khaw of SBIC-Nikon Imaging Center for assistance with fluorescence microscopy.

1. Agarwal AK, Garg A. Seipin: a mysterious protein. *Trends Mol Med* 2004; **10**: 440–444.
2. Ito D, Suzuki N. Molecular pathogenesis of seipin/BSCL2-related motor neuron diseases. *Ann Neurol* 2007; **61**: 237–250.
3. Ito D, Fujisawa T, Iida H, Suzuki N. Characterization of Seipin/BSCL2, a protein associated with spastic paraplegia 17. *Neurobiol Dis* 2008; **30**: 226–277.
4. Lundin C, Nordström R, Wagner K, Windpassinger C, Andersson H, von Heijne G *et al*. Membrane topology of the human seipin protein. *FEBS Lett* 2006; **580**: 2281–2284.
5. Berardinelli W. An undiagnosed endocrinometabolic syndrome: report of 2 cases. *J Clin Endocrinol Metab* 1954; **14**: 193–204.
6. Seip M, Trygstad O. Generalized lipodystrophy, congenital and acquired (lipotrophy). *Acta Paediatr Suppl* 1996; **413**: 2–28.
7. Patel H, Hart PE, Warner TT, Houlston RS, Patton MA, Jeffery S *et al*. The Silver syndrome variant of hereditary spastic paraplegia maps to chromosome 11q12–q14, with evidence for genetic heterogeneity within this subtype. *Am J Hum Genet* 2001; **69**: 209–215.
8. Windpassinger C, Auer-Grumbach M, Irobi J, Patel H, Petek E, Horl G *et al*. Heterozygous missense mutations in BSCL2 are associated with distal hereditary motor neuropathy and Silver syndrome. *Nat Genet* 2004; **36**: 271–276.
9. Auer-Grumbach M, Schlotter-Weigel B, Lochmuller H, Strobl-Wildemann G, Auer-Grumbach P, Fischer R *et al*. Phenotypes of the N88S Berardinelli-Seip congenital lipodystrophy 2 mutation. *Ann Neurol* 2005; **57**: 415–424.
10. Irobi J, Van den Bergh P, Merlini L, Verellen C, Van Maldergem L, Dierick I *et al*. The phenotype of motor neuropathies associated with BSCL2 mutations is broader than Silver syndrome and distal HMN type V. *Brain* 2004; **127**: 2124–2130.
11. Auer-Grumbach M, Löscher WN, Wagner K, Petek E, Komer E, Offenbacher H *et al*. Phenotypic and genotypic heterogeneity in hereditary motor neuropathy type V: a clinical, electrophysiological and genetic study. *Brain* 2000; **123**: 1612–1623.
12. Ito D, Suzuki N. Seipin/BSCL2-related motor neuron disease, seipinopathy is a novel conformational disease associated with endoplasmic reticulum stress. *Clinical Neurol* 2007; **47**: 329–335.
13. Yagi T, Ito D, Nihei Y, Ishihara T, Suzuki N. N88S seipin mutant transgenic mice develop features of seipinopathy/BSCL2-related motor neuron disease via endoplasmic reticulum stress. *Hum Mol Genet* 2011; **20**: 3831–3840.
14. Ito D, Suzuki N. Seipinopathy: a novel endoplasmic reticulum stress-associated disease. *Brain* 2009; **132**: 8–15.
15. Dierick I, Baets J, Irobi J, Jacobs A, De Vriendt E, Deconinck T *et al*. Relative contribution of mutations in genes for autosomal dominant distal hereditary motor neuropathies: a genotype–phenotype correlation study. *Brain* 2008; **131**: 1217–1227.
16. Han W, Rhee JS, Maximov A, Lin W, Hammer RE, Rosenmund C *et al*. C-terminal ECFP fusion impairs synaptotagmin 1 function: crowding out synaptotagmin 1. *J Biol Chem* 2005; **280**: 5089–5100.
17. Gordon JW, Chesa PG, Nishimura H, Rettig WJ, Maccari JE, Endo T *et al*. Regulation of Thy-1 gene expression in transgenic mice. *Cell* 1987; **50**: 445–452.
18. Ikeda M, Kawarabayashi T, Harigaya Y, Sasaki A, Yamada S, Matsubara E *et al*. Motor impairment and aberrant production of neurochemicals in human alpha-synuclein A30P + A53T transgenic mice with alpha-synuclein pathology. *Brain Res* 2009; **1250**: 232–241.
19. Oddo S, Caccamo A, Shepherd JD, Murphy MP, Golde TE, Kaye R *et al*. Triple-transgenic model of Alzheimer's disease with plaques and tangles: intracellular Abeta and synaptic dysfunction. *Neuron* 2003; **39**: 409–421.
20. Crawley JN. Behavioral phenotyping of transgenic and knockout mice: experimental design and evaluation of general health, sensory functions, motor abilities, and specific behavioral tests. *Brain Res* 1999; **835**: 18–26.
21. Brugman F, Scheffer H, Schelhaas HJ, Nillesen WM, Wokke JH, van de Warrenburg BP *et al*. Seipin/BSCL2 mutation screening in sporadic adult-onset upper motor neuron syndromes. *J Neurol* 2009; **256**: 824–826.
22. Wood JD, Beaujeux TP, Shaw PJ. Protein aggregation in motor neuron disorders. *Neuropathol Appl Neurobiol* 2003; **29**: 529–545.
23. Buijini LI, Miller TM, Cleveland DW. Unraveling the mechanisms involved in motor neuron degeneration in ALS. *Annu Rev Neurosci* 2004; **27**: 723–749.
24. Cleveland DW, Rothstein JD. From Charcot to Lou Gehrig: deciphering selective motor neuron death in ALS. *Nat Rev Neurosci* 2001; **2**: 806–819.
25. Martin LJ, Liu Z, Chen K, Price AC, Pan Y, Swaby JA *et al*. Motor neuron degeneration in amyotrophic lateral sclerosis mutant superoxide dismutase-1 transgenic mice: mechanisms of mitochondrial pathology and cell death. *J Comp Neurol* 2007; **500**: 20–46.
26. Friesen A, Kaltschmidt JA, Ladle DR, Sigris M, Jessell TM, Arber S. Gamma and alpha motor neurons distinguished by expression of transcription factor Err3. *Proc Natl Acad Sci USA* 2009; **106**: 13588–13593.
27. Ito D, Suzuki N. Seipinopathy: a novel endoplasmic reticulum stress-associated disease. *Brain* 2009; **132**: 8–15.

28. Zhang K, Kaufman RJ. From endoplasmic-reticulum stress to the inflammatory response. *Nature* 2008; **454**: 455–462.
29. Salminen A, Kauppinen A, Suuronen T, Kaariranta K, Ojala J. ER stress in Alzheimer's disease: a novel neuronal trigger for inflammation and Alzheimer's pathology. *J Neuroinflamm* 2009; **6**: 41.
30. Luo S, Baumeister P, Yang S, Abcouwer SF, Lee AS. Induction of Grp78/BIP by translational block: activation of the Grp78 promoter by ATF4 through and upstream ATF/CRE site independent of the endoplasmic reticulum stress elements. *J Biol Chem* 2003; **278**: 37375–37385.
31. Klionsky DJ, Emr SD. Autophagy as a regulated pathway of cellular degradation. *Science* 2000; **290**: 1717–1721.
32. Ravikumar B, Vacher C, Berger Z, Davies JE, Luo S, Oroz LG *et al*. Inhibition of mTOR induces autophagy and reduces toxicity of polyglutamine expansions in fly and mouse models of Huntington disease. *Nat Genet* 2004; **36**: 585–595.
33. Tarabal O, Caldero J, Casas C, Oppenheim RW, Esquerda JE. Protein retention in the endoplasmic reticulum, blockade of programmed cell death and autophagy selectively occur in spinal cord motoneurons after glutamate receptor-mediated injury. *Mol Cell Neurosci* 2005; **29**: 283–298.
34. Hariri M, Millane G, Guimond MP, Guay G, Dennis JW, Nabi IR. Biogenesis of multilamellar bodies via autophagy. *Mol Biol Cell* 2000; **11**: 255–268.
35. Nixon RA, Wegiel J, Kumar A, Yu WH, Peterhoff C, Cataldo A *et al*. Extensive involvement of autophagy in Alzheimer disease: an immuno-electron microscopy study. *J Neuropathol Exp Neurol* 2005; **64**: 113–122.
36. Martin LJ, Chen K, Liu Z. Adult motor neuron apoptosis is mediated by nitric oxide and Fas death receptor linked by DNA damage and p53 activation. *J Neurosci* 2005; **25**: 6449–6459.
37. Martin LJ. Neuronal death in amyotrophic lateral sclerosis is apoptosis: possible contribution of a programmed cell death mechanism. *J Neuropathol Exp Neurol* 1999; **58**: 459–471.
38. Mourelatos Z, Adler H, Hirano A, Donnerfeld H, Gonatas JO, Gonatas NK. Fragmentation of the Golgi apparatus of motor neurons in amyotrophic lateral sclerosis revealed by organelle-specific antibodies. *Proc Natl Acad Sci USA* 1990; **87**: 4393–4395.
39. Mourelatos Z, Hirano A, Rosenquist AC, Gonatas NK. Fragmentation of the Golgi apparatus of motor neurons in amyotrophic lateral sclerosis (ALS). Clinical studies in ALS of Guam and experimental studies in deafferented neurons and in beta,beta'-iminodipropionitrile axonopathy. *Am J Pathol* 1994; **144**: 1288–1300.
40. Fujita Y, Okamoto K, Sakurai A, Amari M, Nakazato Y, Gonatas NK. Fragmentation of the Golgi apparatus of Betz cells in patients with amyotrophic lateral sclerosis. *J Neurol Sci* 1999; **163**: 81–85.
41. Fujita Y, Okamoto K. Golgi apparatus of the motor neurons in patients with amyotrophic lateral sclerosis and in mice models of amyotrophic lateral sclerosis. *Neuropathology* 2005; **25**: 388–394.
42. Wong E, Cuervo AM. Autophagy gone awry in neurodegenerative diseases. *Nat Neurosci* 2010; **13**: 805–811.
43. Li L, Zhang X, Le W. Altered macroautophagy in the spinal cord of SOD1 mutant mice. *Autophagy* 2008; **4**: 290–293.
44. Sasaki S. Autophagy in spinal cord motor neurons in sporadic amyotrophic lateral sclerosis. *J Neuropathol Exp Neurol* 2011; **70**: 349–359.
45. Kabuta T, Suzuki Y, Wada K. Degradation of amyotrophic lateral sclerosis-linked mutant Cu,Zn-superoxide dismutase proteins by macroautophagy and the proteasome. *J Biol Chem* 2006; **281**: 30524–30533.
46. Pattingre S, Tassa A, Qu X, Garuti R, Liang XH, Mizushima N *et al*. Bcl-2 antiapoptotic proteins inhibit Beclin 1-dependent autophagy. *Cell* 2005; **122**: 927–939.
47. Yu WH, Cuervo AM, Kumar A, Peterhoff CM, Schmidt SD, Lee JH *et al*. Macroautophagy – a novel beta-amyloid peptide-generating pathway activated in Alzheimer's disease. *J Cell Biol* 2005; **171**: 87–98.
48. Chu CT. Autophagic stress in neuronal injury and disease. *J Neuropathol Exp Neurol* 2006; **65**: 423–432.
49. Levine B, Kroemer G. Autophagy in the pathogenesis of disease. *Cell* 2008; **132**: 27–42.
50. Hogan B, Beddington R, Costantini F, Lacy E. *Manipulating the Mouse Embryo: A Laboratory Manual*. 2nd edn. Cold Spring Harbor Laboratory Press: Cold Spring Harbor, NY, USA, 1994.
51. Yang G, Lim CY, Li C, Xiao X, Radda GK, Li C *et al*. FoxO1 inhibits leptin regulation of pro-opiomelanocortin promoter activity by blocking STAT3 interaction with specificity protein 1. *J Biol Chem* 2009; **284**: 3719–3727.
52. Lou PH, Yang G, Huang L, Cui Y, Pourbahrami T, Radda GK *et al*. Reduced body weight and increased energy expenditure in transgenic mice over-expressing soluble leptin receptor. *PLoS One* 2010; **5**: e11669.
53. Senechal Y, Kelly PH, Dev KK. Amyloid precursor protein knockout mice show age-dependent deficits in passive avoidance learning. *Behav Brain Res* 2008; **186**: 126–132.
54. Hamers FP, Lankhorst AJ, van Laar TJ, Veldhuis WB, Gispen WH. Automated quantitative gait analysis during overground locomotion in the rat: its application to spinal cord contusion and transection injuries. *J Neurotrauma* 2001; **18**: 187–201.
55. Lance-Jones C. Motoneuron cell death in the developing lumbar spinal cord of the mouse. *Brain Res* 1982; **256**: 473–479.



Cell Death and Disease is an open-access journal published by Nature Publishing Group. This work is licensed under a Creative Commons Attribution-NonCommercial-ShareAlike 3.0 Unported License. To view a copy of this license, visit <http://creativecommons.org/licenses/by-nc-sa/3.0/>

Supplementary Information accompanies this paper on Cell Death and Disease website (<http://www.nature.com/cddis>)